

# Energy and Electron Transfer from Fluorescent Mesostructured Organosilica Framework to Guest Dyes

Norihiro Mizoshita,<sup>†,‡</sup> Ken-ichi Yamanaka,<sup>†,‡</sup> Satoru Hiroto,<sup>§</sup> Hiroshi Shinokubo,<sup>§</sup> Takao Tani,<sup>†,‡</sup> and Shinji Inagaki<sup>\*,†,‡</sup>

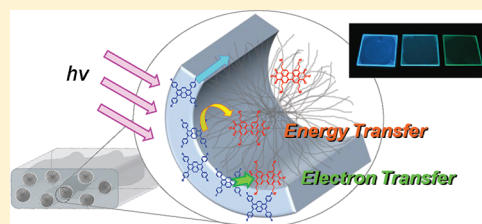
<sup>†</sup>Toyota Central Research and Development Laboratories, Incorporated, Nagakute, Aichi 480-1192, Japan

<sup>‡</sup>Core Research for Evolutional Science and Technology (CREST), Japan Science and Technology Agency (JST), Kawaguchi, Saitama 332-0012, Japan

<sup>§</sup>Department of Applied Chemistry, Graduate School of Engineering, Nagoya University, Chikusa, Nagoya 464-8603, Japan

## Supporting Information

**ABSTRACT:** Energy and electron transfer from frameworks of nanoporous or mesostructured materials to guest species in the nanochannels have been attracting much attention because of their increasing availability for the design and construction of solid photofunctional systems, such as luminescent materials, photovoltaic devices, and photocatalysts. In the present study, energy and electron-transfer behavior of dye-doped periodic mesostructured organosilica films with different host–guest arrangements were systematically examined. Fluorescent tetraphenylpyrene (TPPy)–silica mesostructured films were used as a host donor. The location of guest perylene bisimide (PBI) dye molecules, acting as an acceptor, could be controlled on the basis of the molecular design of the PBI substituent groups. PBI dyes with bulky substituents and polar anchoring groups were located at the pore surface with low self-aggregation, which induced efficient energy or electron transfer because of the close host–guest arrangement. However, PBI dye with bulky and hydrophobic substituents was located in the center of template surfactant micelles; the fluorescence emission from the host TPPy groups was hardly quenched when the host–guest distance was longer than the critical Förster radius (ca. 4.5 nm). The relationship between the energy or electron-transfer efficiency and the location of guest species in the channels of mesostructured organosilica was first revealed by molecular design of the PBI substituents.



## INTRODUCTION

Periodic mesostructured and mesoporous organosilicas prepared by surfactant-directed polycondensation of bridged organosilane precursors  $\{R[Si(OR')_3]_n\}$ , where  $n \geq 2$ ,  $R$  = organic bridging group, and  $R' = Me, Et, \text{etc.}\}$  are a new class of inorganic–organic hybrid materials with organic-functionalized frameworks.<sup>1–7</sup> A variety of organic bridging groups ( $R$ ), ranging from aliphatic and aromatic groups to heterocyclic compounds, have been used to tailor the functionalities of the silica-based pore walls.<sup>1–7</sup> This type of mesostructured material allows for different organic chromophores to be located in two spatially separated regions, i.e., in the framework and in the mesochannels. Appropriate selection of host framework organic groups ( $R$ ) and guest materials induces energy and electron transfer between the pore walls and the guest molecules located in the mesochannels upon photoexcitation.

Recently, the use of energy and electron transfer between pore walls and mesochannels has broadened potential applications of periodic mesostructured and mesoporous organosilicas, such as light-harvesting antenna properties,<sup>8,9</sup> color-tunable fluorescence emission,<sup>10–12</sup> photocatalytic hydrogen evolution,<sup>13</sup> and enhanced photocatalytic  $CO_2$  reduction.<sup>14</sup> Highly efficient Förster resonance energy transfer (FRET) from the pore walls to guest dyes has been reported for coumarin-

doped mesoporous biphenyl–silica hybrids.<sup>8</sup> The energy-transfer efficiency for this host–guest system was almost 100%, even at a low coumarin concentration of 0.8 mol % to the biphenyl units. The coumarin dye was thought to be located in the proximity of the hydrophilic pore wall to result in such a high FRET efficiency. Periodic mesostructured films doped with fluorescent dyes have also exhibited highly efficient and color-tunable photoluminescence because of FRET from the organosilica pore walls to the guest dyes.<sup>10,11</sup> Appropriate dispersion of the fluorescent dye dopants in the mesochannels enabled effective tuning of the emission colors and high fluorescence quantum yields. On the other hand, photo-induced electron transfer has been observed for hydrogen evolution systems, where charge-transfer sites are formed by covalently attaching an electron-receptive viologen onto the pore wall surface of biphenyl–silica mesoporous materials.<sup>13</sup> For potential applications, the distance and arrangement of the energy/electron donors and acceptors are of great importance to induce significant energy/electron transfer between the pore walls (hosts) and guests. Teramae and colleagues examined the

Received: November 24, 2011

Revised: January 16, 2012

Published: January 17, 2012

local environments of coumarin dyes in mesostructured silica-surfactant nanocomposites by measuring the time-dependent fluorescence spectral shift.<sup>15</sup> Zink and colleagues studied the precise energy and electron-transfer behavior in multi-doped mesostructured thin films.<sup>16</sup> However, there has been no systematic study on the energy and electron-transfer behavior of dye-doped periodic mesostructured organosilicas with different donor-acceptor arrangements.

In the present study, we have examined the influence of the dispersion state and location of guest acceptor molecules on the energy or electron-transfer behavior in periodic mesostructured organosilica films by systematically changing the donor-acceptor arrangement based on molecular design of the acceptor substituent groups. Blue-fluorescent tetraphenylpyrene (TPPy)-silica mesostructured films<sup>11</sup> were selected as host (energy/electron donor) materials, and perylene bisimide (PBI) dyes were selected as guest (acceptor) molecules (Figure 1). Figure 2 shows a schematic illustration of the possible

photochemical processes that occur in the PBI-doped mesostructured films. PBI derivatives exhibit strong absorption in the visible light wavelength region and also have an electron-deficient core; therefore, efficient FRET occurs when the guest PBI dyes are located within the critical Förster radius of the TPPy-PBI (donor-acceptor) pairs (Figure 2C); photo-induced electron transfer can also occur when a close host-guest arrangement is realized at the pore wall surface (Figure 2B). For induction of such a host-guest interaction, four PBI dyes 1-4 were synthesized with substituents ( $R^1$  and  $R^2$ ) that possess different functionality and bulkiness on the imide groups and 2, 5, 8, and 11 positions (Figure 1). Although chemical modification of PBIs had relied on N substitution of imide groups or transformation of the bay area (1, 6, 7, and 12 positions),<sup>17</sup> selective functionalization of the 2, 5, 8, and 11 positions of PBIs has recently been exploited by Shinokubo and co-workers.<sup>18</sup> This new synthetic method has enabled the systematic synthesis of PBI dyes with various substituents. The obtained PBI dyes were incorporated into TPPy-silica mesostructured films containing non-ionic template surfactants. Energetic and electronic host-guest communications in PBI-doped TPPy-silica mesostructured films were examined on the basis of their fluorescence emission and quenching behavior.

## EXPERIMENTAL SECTION

**Materials and Methods.** All reagents and solvents were purchased from Aldrich, Gelest, and Tokyo Chemical Industry and used without further purification. Poly(ethylene oxide)-*block*-poly(propylene oxide)-*block*-poly(ethylene oxide) (PEO-PPO-PEO) triblock co-polymer (EO<sub>20</sub>-PO<sub>70</sub>-EO<sub>20</sub>, P123, Aldrich) and poly(ethylene oxide) octadecyl ether (EO<sub>10</sub>-C<sub>18</sub>H<sub>37</sub>, Brij76, Aldrich) were used as a non-ionic template surfactant. <sup>1</sup>H and <sup>13</sup>C nuclear magnetic resonance (NMR) spectra were measured using a Jeol JNM-ECX400P spectrometer. Mass spectra were recorded on a Bruker Daltonics Autoflex mass spectrometer with matrix-assisted laser desorption/ionization (MALDI). X-ray diffraction (XRD) measurements were performed using Cu K $\alpha$  radiation (Rigaku RINT-TTR, 50 kV, 300 mA). Ultraviolet-visible (UV-vis) absorption spectra were measured using a Jasco V-670 spectrometer. Fluorescence spectra were obtained with a Jasco FP-6500 spectrometer. Femtosecond time-resolved absorption spectra were measured using a pump-probe technique (CDP, ExciPro). The output of a mode-locked Ti:Sapphire oscillator (Coherent, Vitesse) was pumped by the second harmonic generation (SHG) of a continuous wave Nd<sup>3+</sup>:YVO<sub>4</sub> laser (Coherent, Verdi) and was amplified with a regenerative amplifier (Coherent, Legend) pumped by a Nd<sup>3+</sup>:YLF laser (Coherent, Evolution). The output of the amplifier [2.4 W, 100 fs full width at half maximum (fwhm), 1 kHz] was divided into two parts. One part was converted to the Signal (1570 nm) using an optical parametric amplifier (OPA) system (Coherent, OPerA). The Signal light was coincident with the fundamental light in a 0.5 mm thick  $\beta$ -BaB<sub>2</sub>O<sub>4</sub> (BBO) crystal for sum frequency generation (SFG), where the SFG process converts the Signal and fundamental light into SFG. The SFG pulse (530 nm) was directed through a half-wave plate and then used as a pump light after the repetition rate was modulated to 0.5 kHz using a chopper. The relative polarization between the excitation and probe pulses was fixed at the magic angle (54.7°). The other part of the amplified Ti:Sapphire output was directed through an optical delay circuit with a computer-controlled stepping motor and then focused into a 5 mm H<sub>2</sub>O cell to generate a white-light continuum. The white light was collimated with an achromatic lens and sent through a filter (Hoya, C5000) for elimination of the fundamental light. A small portion of the collimated white light was used as the reference light, and the residual light was focused on the sample. A rotating sample holder was used. The transmitted probe light and the reference light were detected with a polychromator (Solartii, MS3501I) and a multichannel photodiode array detector. The spectral data at every fixed delay were averaged

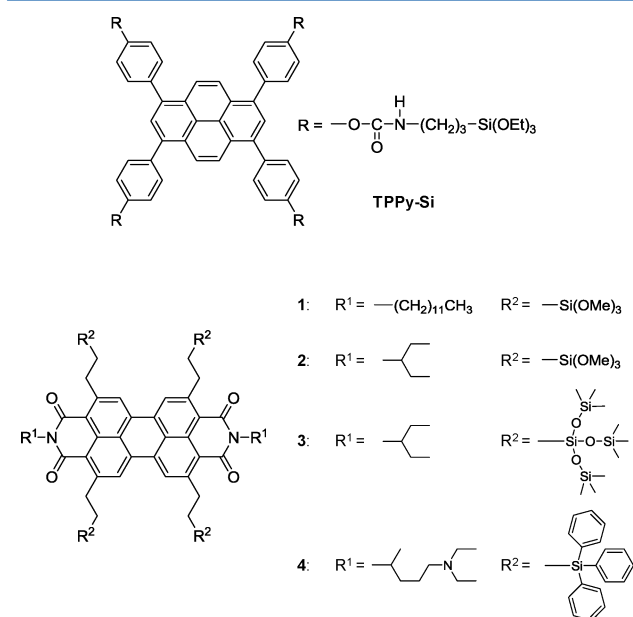


**Figure 1.** Chemical structures of TPPy-derived organosilane precursor TPPy-Si and PBI dyes 1-4.

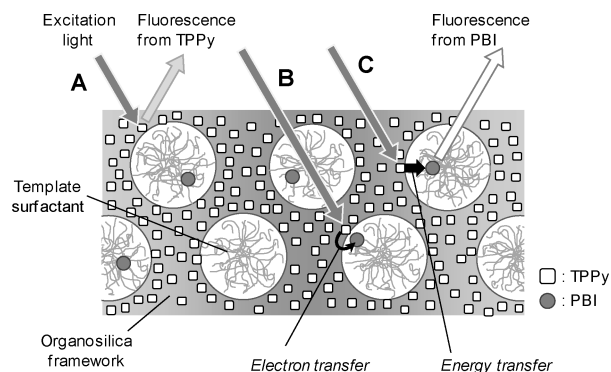
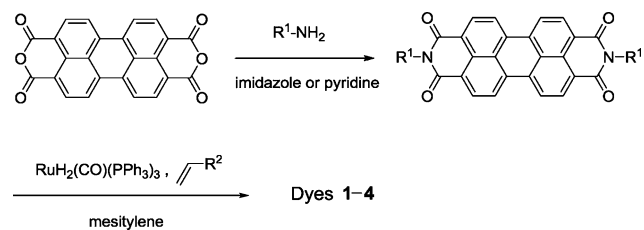


**Figure 2.** Possible photochemical processes in mesostructured TPPy-silica films containing PBI dyes upon photoexcitation of the TPPy moieties: (A) fluorescence emission from the TPPy moiety, (B) photo-induced electron transfer from TPPy to PBI, and (C) energy transfer from TPPy to PBI, followed by fluorescence emission of PBI.

over 500 pulse shots. The chirp structure of the probe light was corrected by measuring the optical Kerr signal.<sup>19</sup> The time resolution of this system was less than 300 fs. The excitation wavelength (530 nm) was adjusted to the absorption band of PBI acceptor molecules to detect the direct electron-transfer process from the TPPy moiety to the excited PBI chromophore.

**Synthesis of Organic Components.** Organosilane precursor TPPy–Si and dye 2 (Figure 1) were synthesized using previously reported procedures.<sup>11,18a</sup> PBI dyes 1, 3, and 4 with different substituents were synthesized according to the route shown in Scheme 1.

**Scheme 1. Synthetic Route for PBI Dyes 1–4**



*N,N'*-Didodecyl-2,5,8,11-tetrakis[2-(trimethoxysilyl)ethyl]perylene-3,4,9,10-tetracarboxylic Acid Bisimide (**1**). A mixture of *N,N'*-didodecylperylene-3,4,9,10-tetracarboxylic acid bisimide (72.3 mg, 0.10 mmol), trimethoxyvinylsilane (220 mg, 1.5 mmol), mesitylene (0.3 mL), and  $\text{RuH}_2(\text{CO})(\text{PPh}_3)_3$  (5.5 mg, 0.006 mmol) was stirred at 160 °C for 48 h. The reaction mixture was passed through a pad of gel permeation chromatography (GPC) gel (Bio-Rad Bio-Beads S-X1) with tetrahydrofuran (THF). The concentration of the solution under reduced pressure provided the product (125.2 mg, 95%). <sup>1</sup>H NMR ( $\text{CDCl}_3$ , ppm)  $\delta$ : 0.88 (t,  $J = 7.0$  Hz, 6H), 1.23 (m, 8H), 1.26 (m, 32H), 1.40 (m, 4H), 1.73 (m, 4H), 3.63 (m, 8H), 3.68 (s, 36H), 4.19 (t,  $J = 7.5$  Hz, 4H), 8.43 (s, 4H). <sup>13</sup>C NMR ( $\text{CDCl}_3$ , ppm)  $\delta$ : 10.8, 14.2, 22.7, 27.3, 28.1, 29.4, 29.7, 30.4, 31.9, 40.4, 50.7, 119.5, 124.3, 126.8, 131.8, 133.2, 152.2, 163.2. MS (MALDI,  $m/z$ ): calcd for  $\text{C}_{68}\text{H}_{106}\text{N}_2\text{O}_{16}\text{Si}_4$  1318.66;  $[\text{M}]^+$ , found 1318.66.

*N,N'*-Bis(3-pentyl)-2,5,8,11-tetrakis[2-(tris(trimethylsilyloxy)silyl)ethyl]perylene-3,4,9,10-tetracarboxylic Acid Bisimide (**3**). A mixture of *N,N'*-bis(3-pentyl)perylene-3,4,9,10-tetracarboxylic acid bisimide (0.265 g, 0.50 mmol), tris(trimethylsilyloxy)vinylsilane (2.42 g, 7.50 mmol), mesitylene (5.0 mL), and  $\text{RuH}_2(\text{CO})(\text{PPh}_3)_3$  (46.0 mg, 0.05 mmol) was stirred at 160 °C for 48 h. The reaction mixture was diluted with hexane (5 mL) and separated on silica gel using a hexane/chloroform (3:1, v/v) eluent to afford the product (0.34 g, 37%). <sup>1</sup>H NMR ( $\text{CDCl}_3$ , ppm)  $\delta$ : 0.15 (m, 108H), 0.91 (t,  $J = 7.1$  Hz, 12H), 1.01 (m, 8H), 1.94 (m, 4H), 2.32 (m, 4H), 3.51 (m, 8H), 5.11 (m, 2H), 8.32 (s, 4H). <sup>13</sup>C NMR ( $\text{CDCl}_3$ , ppm)  $\delta$ : 1.9, 11.4, 16.2, 25.1, 31.1, 57.2, 120.1, 124.2, 126.2, 132.0, 132.9, 152.7, 164.1. MS (MALDI,  $m/z$ ): calcd for  $\text{C}_{78}\text{H}_{150}\text{N}_2\text{O}_{16}\text{Si}_{16}$  1818.73;  $[\text{M}]^+$ , found 1818.73.

*N,N'*-Bis(4-diethylamino-1-methylbutyl)perylene-3,4,9,10-tetracarboxylic Acid Bisimide. 2-Amino-5-diethylaminopentane (3.17 g, 20.0 mmol) was added to a mixture of perylene-3,4,9,10-tetracarboxylic dianhydride (1.57 g, 4.00 mmol) and imidazole (10.0 g) and stirred at 160 °C for 16 h. After cooling to room temperature, ethanol (100 mL) was added, and the mixture was stirred for 0.5 h. The resultant precipitate was collected by suction filtration, washed with ethanol, and dried under reduced pressure to afford the product as a red solid (2.60 g, 97%). <sup>1</sup>H NMR ( $\text{CDCl}_3$ , ppm)  $\delta$ : 0.95 (t,  $J = 7.1$  Hz, 12H), 1.40 (m, 2H), 1.51 (m, 2H), 1.61 (d,  $J = 7.0$  Hz, 6H), 1.90 (m, 2H), 2.23 (m, 2H), 2.39–2.50 (m, 12H), 5.30 (m, 2H), 8.53 (d,  $J = 8.1$  Hz, 4H), 8.60 (d,  $J = 8.1$  Hz, 4H).

*N,N'*-Bis(4-diethylamino-1-methylbutyl)-2,5,8,11-tetrakis[2-(triphenylsilyl)ethyl]perylene-3,4,9,10-tetracarboxylic Acid Bisimide (**4**). A mixture of *N,N'*-bis(4-diethylamino-1-methylbutyl)perylene-3,4,9,10-tetracarboxylic acid bisimide (0.50 g, 0.74 mmol), triphenylvinylsilane (3.18 g, 11.1 mmol), mesitylene (10.0 mL), and  $\text{RuH}_2(\text{CO})(\text{PPh}_3)_3$  (64.4 mg, 0.07 mmol) was stirred at 160 °C for 22

h. The reaction mixture was diluted with chloroform (5 mL) and separated on silica gel using a chloroform/ethanol (10:1, v/v) eluent to afford the product (1.18 g, 88%). <sup>1</sup>H NMR ( $\text{CDCl}_3$ , ppm)  $\delta$ : 0.91 (t,  $J = 7.1$  Hz, 12H), 1.43 (m, 2H), 1.51 (m, 2H), 1.61 (d,  $J = 7.0$  Hz, 6H), 1.95 (m, 10H), 2.23 (m, 2H), 2.39–2.47 (m, 12H), 3.64 [t(br),  $J = 8.1$  Hz, 8H], 5.29 (m, 2H), 7.28–7.35 (m, 36H), 7.63 (m, 24H), 7.85 (s, 4H). <sup>13</sup>C NMR ( $\text{CDCl}_3$ , ppm)  $\delta$ : 11.6, 14.8, 18.5, 24.9, 31.6, 32.0, 46.9, 49.4, 52.9, 120.1, 124.2, 126.6, 127.8, 129.4, 131.7, 132.7, 135.1, 135.7, 152.0, 163.7. MS (MALDI,  $m/z$ ): calcd for  $\text{C}_{122}\text{H}_{120}\text{N}_4\text{O}_4\text{Si}_4$  1817.85;  $[\text{M} + \text{H}]^+$ , found 1817.85.

**Preparation of Organosilica Films.** The TPPy-based precursor TPPy–Si (150 mg), tetraethoxysilane (150 mg), and non-ionic template surfactant (200 mg) were dissolved in 8.0 mL of a 1:1 (w/w) mixture of THF and ethanol, followed by the addition of 2 M hydrochloric acid (40  $\mu\text{L}$ ) and deionized water (200  $\mu\text{L}$ ). The total amount of solution was adjusted to 10.0 mL using a volumetric flask ( $[\text{TPPy-Si}] = 9.6$  mM). The sol mixtures were stirred at room temperature for 24 h. Appropriate amounts of dyes (0–10.0 mol % ratios to the amount of TPPy units) were added to the sol solution using a 9.6 mM solution of dyes in THF, and then dye-doped organosilica thin films were prepared by spin-coating the solutions onto quartz substrates (4000 rpm for 30 s) and drying under reduced pressure at room temperature for 24 h. The organosilica films were stored in the dark prior to optical measurements.

## RESULTS AND DISCUSSION

The PBI dyes 1–4 were successfully synthesized by imidation of perylene tetracarboxylic dianhydride with aliphatic amines and subsequent Ru-catalyzed 2, 5, 8, and 11 alkylation using vinylsilane compounds (Scheme 1).  $\text{R}^1$  and  $\text{R}^2$  substituents were selected to tune the polarity and bulkiness of the PBI dyes (Figure 1). PBI dyes 1 and 2 have trimethoxysilyl moieties as  $\text{R}^2$  to anchor on the pore wall surface. Linear and branched alkyl chains were appended for dyes 1 and 2, respectively, to examine the steric effect of  $\text{R}^1$ . Dye 3 possesses the same branched  $\text{R}^1$  as dye 2, but the  $\text{R}^2$  is a bulky and hydrophobic tris(trimethylsilyloxy)silyl group; therefore, dye 3 is an entirely hydrophobic molecule designed to suppress self-aggregation. Dye 4 has polar amino groups as  $\text{R}^1$  and bulky triphenylsilyl groups as  $\text{R}^2$ . In this dye, the  $\text{R}^1$  amino group, which is protonated in an acidic sol–gel process, is a polar anchoring group for the silica-based pore walls. A rigid aromatic  $\text{R}^2$  substituent was introduced to suppress self-aggregation of the PBI moieties and to promote segregation of the dye molecules from micellar cores consisting of aliphatic chains of the template surfactants.

Solutions of the PBI dyes 1–4 in THF exhibited similar UV–vis absorption and fluorescence spectra, with absorption maximum wavelengths ( $\lambda_{\text{max}}$ ) of 520–524 nm and fluorescence wavelengths of 536–544 nm, because of the same chemical structure of the PBI chromophore (see Figure S1 of the Supporting Information). Figure 3 shows absorption and fluorescence spectra of a host TPPy–silica mesostructured film containing non-ionic surfactant P123 as a template (denoted as P123–TPPy)<sup>11</sup> and a solution of PBI dye 2 in THF. The large overlap of the fluorescence spectrum of P123–TPPy (curve B) and the absorption spectrum of the PBI dye (curve C) is preferable for efficient FRET from the TPPy (donor) to PBI (acceptor) units. The critical Förster radius for the donor–acceptor pair was estimated to be ca. 4.5 nm from the overlap function (see the Supporting Information).<sup>8,20</sup>

Mesostructured P123–TPPy films containing the PBI dyes were prepared on quartz substrates by a spin-coating method. The mesoscale periodicity of the P123–TPPy films observed by XRD measurements was ca. 8.7 nm, as reported in our

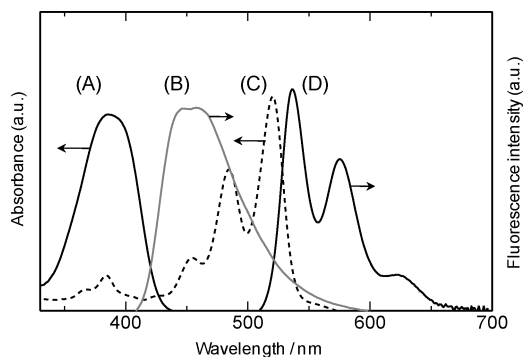


**Figure 3.** UV-vis absorption and fluorescence spectra of the mesostructured P123-TPPy film (curves A and B) and a dilute solution of PBI dye 2 in THF ( $1.0 \times 10^{-5}$  M) (curves C and D). The excitation wavelengths in curves B and D are 400 and 490 nm, respectively.

previous work (Figure S3b of the Supporting Information).<sup>11</sup> The XRD pattern of the film also showed broad diffractions at  $d = 5.0$  and  $4.3$  nm. These diffractions suggest the formation of a two-dimensional (2D) mesochannel array close to hexagonal packing, because the reciprocal of  $d$ -spacing values is in the ratio of ca.  $1:\sqrt{3}:2$ . UV-vis absorption spectra of the dye-doped P123-TPPy films were measured to examine the dispersion states of the PBI dyes in the films (Figure 4). The

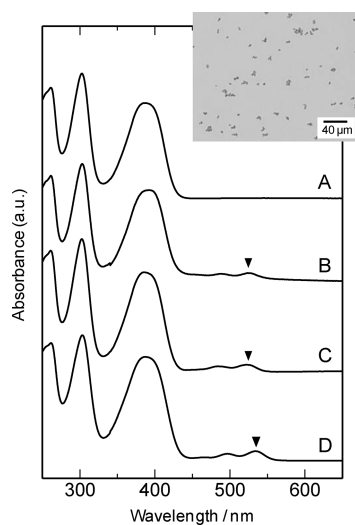


**Figure 4.** UV-vis absorption spectra of P123-TPPy films containing 5 mol % of dyes (A) 1, (B) 2, (C) 3, and (D) 4. The inset shows an optical microscope image of the P123-TPPy/1 film containing micrometer-scale dye aggregates.

P123-TPPy films containing dyes 2–4 (5.0 mol % to the TPPy units) had weak but pronounced absorption bands attributable to the PBI dyes at  $\lambda = 450$ – $560$  nm (curves B, C, and D of Figure 4), and their spectral shapes were similar to those of the dyes in THF solution. In contrast, no absorption band of dye 1 was apparent for the P123-TPPy/1 film (curve A of Figure 4). These results indicate that dyes 2–4 are well-dispersed in the mesostructured films, whereas dye 1 forms large aggregates in the films. Optical microscopy observation of the P123-TPPy/1 film showed the growth of micrometer-scale aggregates of dye 1 (inset of Figure 4). The long linear alkyl chain ( $R^1$ ) of dye 1 seems to exhibit no steric hindrance for dye

aggregation and rather facilitates the self-aggregation by hydrophobic interaction and van der Waals forces. On the other hand,  $\lambda_{\max}$  for the PBI dyes 2–4 doped in the films were 524, 523, and 534 nm, respectively (Figure 4). The larger red shift of  $\lambda_{\max}$  for dye 4 in the P123-TPPy film implies that dye 4 is located in a more polar environment, e.g., in close proximity to organosilica walls, compared to dyes 2 and 3.

The fluorescence emission and quenching behavior of the P123-TPPy films containing PBI dyes was examined upon excitation at  $\lambda = 400$  nm (excitation of the host TPPy units) and 490 nm (direct excitation of the PBI dyes). Figure 5 shows

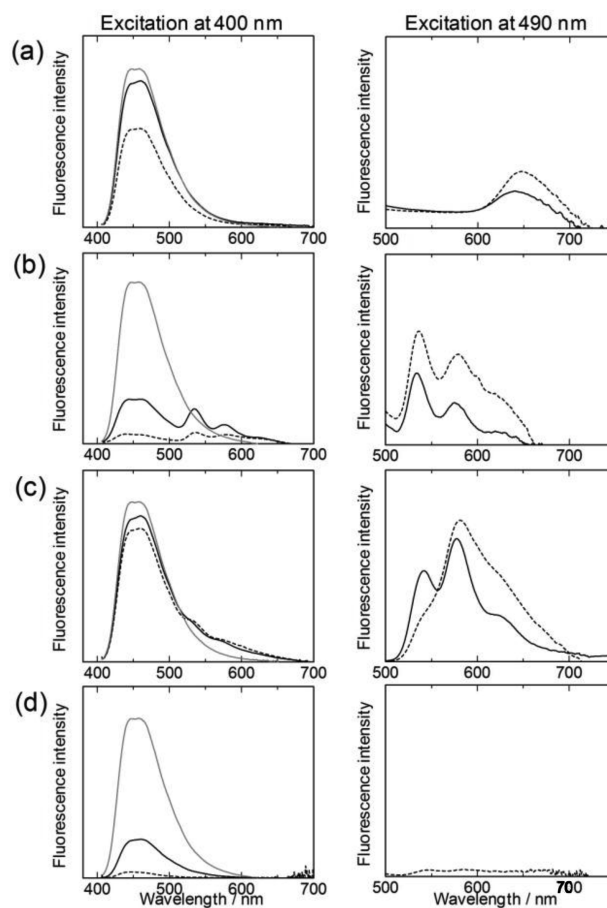


**Figure 5.** Fluorescence spectra of PBI-doped P123-TPPy mesostructured films containing dyes (a) 1, (b) 2, (c) 3, and (d) 4 upon excitation at  $\lambda = 400$  nm (left) and 490 nm (right). Gray solid line, non-doped P123-TPPy; black solid line, 1 mol % dye doping; black broken line, 5 mol % dye doping.

fluorescence spectra of the mesostructured films containing 0, 1.0, and 5.0 mol % of PBI dyes. Figure 6 shows the quenching efficiency ( $1 - I/I_0$ , where  $I$  is the fluorescence intensity at  $\lambda = 450$  nm and  $I_0$  is the fluorescence intensity of the non-doped host film at  $\lambda = 450$  nm)<sup>8,20</sup> of the TPPy chromophore as a function of the doped PBI dye concentration. The fluorescence intensity  $I$  was normalized using the ratio of absorbance of the mesostructured films at  $\lambda = 400$  nm. Strong fluorescence quenching of the host TPPy units by PBI doping was observed for the P123-TPPy/2 and P123-TPPy/4 films (Figure 6). On the other hand, the fluorescence behaviors of the PBI dyes are quite different depending upon the molecular structures of the dyes and the excitation wavelength (Figure 5).

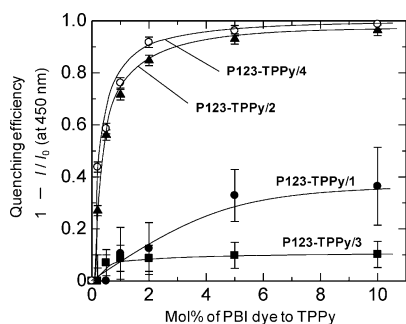


**Figure 6.** Quenching efficiency of the P123-TPPy films doped with PBI dyes.

The P123-TPPy/1 films containing aggregates of dye 1 exhibited slight fluorescence quenching of the TPPy units (Figure 5a). Although micrometer-scale aggregates of dye 1 are contained in the film, a portion of the dye aggregates seems to be finely dispersed and chemically adsorbed on the TPPy-silica framework with the silyl groups of  $R^2$ , which leads to a quenching efficiency of ca. 0.3 (Figure 6). However, no fluorescence emission was observed from dye 1 upon excitation at  $\lambda = 400$  nm, which suggests energy transfer from the TPPy moieties to less emissive dye aggregates. Direct excitation of the dye at  $\lambda = 490$  nm resulted in a broad emission at  $\lambda = 650$  nm, which is attributable to an excimer-band emission from the dye aggregates.

The P123-TPPy/2 films exhibited efficient FRET from the host TPPy to the PBI dye. The fluorescence emission of the TPPy groups upon excitation at  $\lambda = 400$  nm was strongly quenched by doping with dye 2 (Figures 5b and 6), and the fluorescence emission of dye 2 was observed at  $\lambda = 534$  nm (Figure 5b), which is a monomer-band-like emission. In comparison to dye 1, the introduction of a branched alkyl substituent as  $R^1$  had a significant effect on the suppression of dye aggregation, which was supported by the different fluorescence behavior of the PBI dyes upon direct excitation at  $\lambda = 490$  nm (panels a and b of Figure 5). The efficiency of fluorescence quenching of the TPPy groups reached more than 0.9 for 5 mol % dye doping (Figure 6). Efficient fluorescence quenching and energy transfer are realized by chemical adsorption of the PBI dye 2 onto the TPPy-silica framework with the silyl groups of  $R^2$ .

The P123-TPPy/3 films did not exhibit significant fluorescence quenching of the TPPy units (Figure 5c). Upon direct excitation of dye 3 at  $\lambda = 490$  nm, fluorescence emission from PBI was observed with higher emission intensity at  $\lambda = 575$  nm than that at  $\lambda = 540$  nm. The spectral shape indicates that the PBI dye molecules are locally concentrated in the films, exhibiting mixed fluorescence emission from monomeric species and aggregates, while self-quenching by face-to-face association of the PBI cores is suppressed because of the bulky  $R^1$  and  $R^2$  substituents. The strong fluorescence emission from the TPPy units in the P123-TPPy/3 films upon excitation at  $\lambda = 400$  nm suggests that the distance between the host TPPy and the guest PBI chromophores is too far to cause FRET. It is probable that the hydrophobic dye 3 is located at the hydrophobic center of the template surfactant micelles. The critical Förster radius estimated for the TPPy-PBI pair is ca. 4.5 nm; however, the mesoscale periodicity of the host film obtained by XRD measurements is 8.7 nm. Assuming the formation of a 2D hexagonal-like mesostructure, the radius of

the mesocylinder is calculated to be 5.0 nm, which is longer than the critical Förster radius. Moreover, the molecular radius of dye 3 with the large  $R^2$  substituent is ca. 1.1 nm; the distance between the PBI core of dye 3 and the TPPy units embedded within the pore walls could be further elongated by the large substituents ( $R^2$ ) of dye 3.

To examine the effect of the host-guest distance on the FRET from the TPPy bridging groups to dye 3, a TPPy-silica mesostructured film with smaller mesoscale periodicity was prepared using the non-ionic surfactant Brij76 [ $\text{HO}-(\text{CH}_2\text{CH}_2\text{O})_{10}\text{C}_{18}\text{H}_{37}$ ] as a template. The host mesostructured film (Brij76-TPPy) had XRD peaks at  $d = 5.6, 3.2, 2.7, 2.1,$  and 1.9 nm (Figure S3c of the Supporting Information). The reciprocal of the  $d$ -spacing values was in the ratio of  $1:\sqrt{3}:2:\sqrt{7}:3$ , which is typical of a 2D hexagonal arrangement of mesochannels. In comparison to the P123-TPPy film, the Brij76-TPPy film templated by nonpolar hydrocarbon chains seems to have a more ordered periodic mesostructure. The radius of the cylindrical structure was calculated to be 3.3 nm, which was 1.7 nm shorter than that of P123-TPPy. Figure 7a

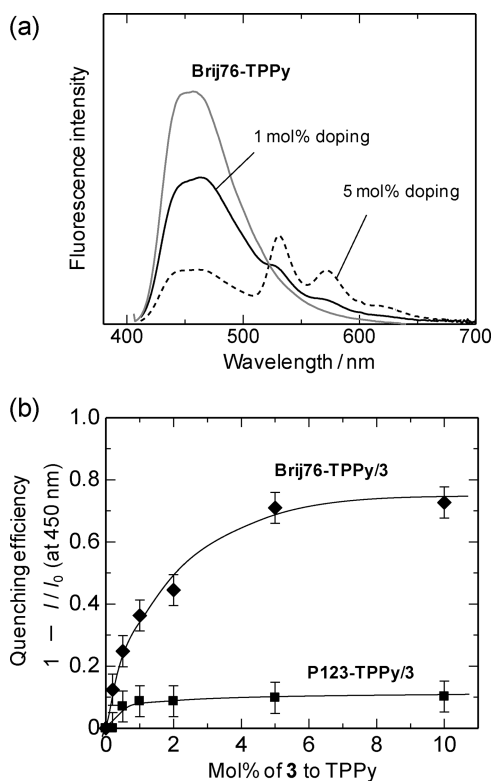


**Figure 7.** (a) Fluorescence spectra of the Brij76-TPPy/3 films upon excitation at  $\lambda = 400$  nm and (b) comparison to fluorescence quenching for mesostructured TPPy-silica films by doping with dye 3.

shows fluorescence spectra for the Brij76-TPPy/3 films upon excitation at  $\lambda = 400$  nm. The fluorescence emission from TPPy was adequately quenched, and the monomer band emission of dye 3 was observed at  $\lambda = 531$  nm, which indicates that FRET occurred in the Brij76-TPPy/3 films. In this case, the fluorescence spectral shape of dye 3 was similar to that of a solution of dye 3 in THF, which differs from the P123-TPPy/3 films (Figure 5c). This is probably because dye 3 with lipophilic trimethylsilyl and 3-pentyl groups is more readily dispersed in the hydrophobic region consisting of Brij76 alkyl chains rather than in the region consisting of polar poly-

(propylene oxide) chains of P123. Figure 7b compares the quenching efficiency, which is equal to the FRET efficiency in this case, of the Brij76–TPPy/3 and P123–TPPy/3 films; the FRET efficiency reached 0.7 for the Brij76–TPPy/3 films. The use of a host mesostructured film with smaller mesoscale periodicity was effective to achieve a large enhancement of the FRET efficiency from the host organosilica framework to guest dye molecules. It should be noted that the FRET efficiency is saturated at ca. 0.7 for Brij76–TPPy/3 and ca. 0.1 for P123–TPPy/3 (Figure 7b), which suggests that hydrophobic dye 3 is selectively incorporated into the center of the surfactant micelles and is not located in the vicinity of the pore walls.

The P123–TPPy/4 films exhibited the most efficient fluorescence quenching of the host TPPy units (Figures 5d and 6). For the PBI dye 4 incorporated into the film, the protonated amino groups functioned as an anchor for the TPPy–silica pore walls and the bulky triphenylsilyl substituents suppressed self-aggregation of the dye molecules. The efficient fluorescence quenching (Figure 6) and the clear UV–vis spectrum of dye 4 with a slight red shift of  $\lambda_{\max}$  (curve D of Figure 4) verified the dispersion of dye 4 in the polar region of the film. However, no fluorescence emission was observed from dye 4 upon excitation at  $\lambda = 400$  or 490 nm (Figure 5d); therefore, the fluorescence quenching most likely corresponds to photo-induced electron transfer from TPPy to PBI.<sup>21</sup> To clarify the formation of electron donor (TPPy)–acceptor (PBI) pairs, dye 4 was incorporated into a P123-templated mesostructured silica film (P123–silica) with no TPPy bridging group (Figure 8).<sup>22</sup> The  $\lambda_{\max}$  of dye 4 in the P123–silica film

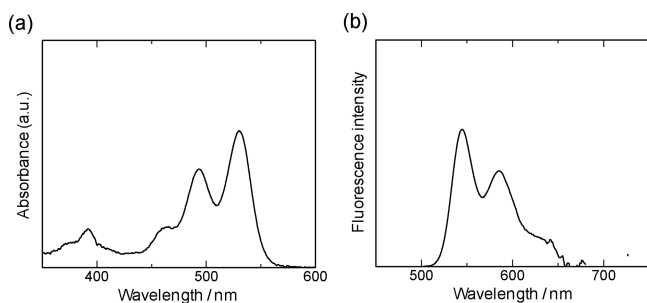


**Figure 8.** (a) UV–vis absorption and (b) fluorescence (excited at  $\lambda = 490$  nm) spectra of dye 4 incorporated into the P123–silica film containing no TPPy units (P123/4 = 100:0.2, w/w).

was 530 nm, which is slightly longer than that in THF solution ( $\lambda_{\max} = 524$  nm). Upon excitation at  $\lambda = 490$  nm, the film exhibited strong fluorescence emission at  $\lambda = 545$  nm attributable to the monomer band emission of dye 4, which confirms that the dye molecules incorporated into the P123–silica film are well-dispersed and highly fluorescent without being quenched by the silica framework. This result conversely verifies the strong electronic interaction of the TPPy units and dye 4 in the P123–TPPy/4 films.

Photo-induced electron transfer in the P123–TPPy/4 films was revealed by time-resolved absorption spectroscopy. Figure 9 shows transient absorption spectra of the P123–TPPy/4 film containing 10 mol % dye 4 after selective excitation of dye 4 at  $\lambda = 530$  nm. The spectra show transient absorption bands around  $\lambda = 700$  and 580 nm, with intense bleaching observed at  $\lambda = 492$  and 531 nm ( $S_0 \rightarrow S_1$  transition of the PBI dye). The broad absorption band around  $\lambda = 700$  nm can be attributed to both the singlet state ( $^1\text{PBI}^*$ ) and anionic radical ( $\text{PBI}^{\bullet-}$ ) of

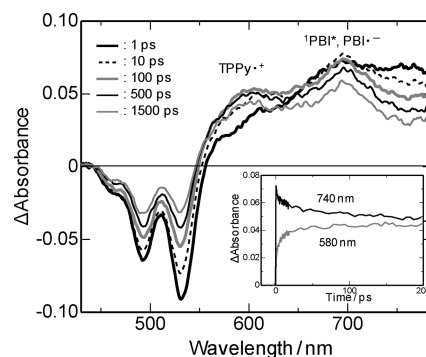


**Figure 9.** Transient absorption spectra of the P123–TPPy/4 film containing 10 mol % dye 4 after laser excitation at  $\lambda = 530$  nm. The inset shows time profiles of  $\Delta$ absorbance at  $\lambda = 580$  and 740 nm.

PBI.<sup>23</sup> An absorption band around  $\lambda = 770$  nm is attributable to excited species of partially formed dye aggregates.<sup>24</sup> On the other hand, the transient absorption band at  $\lambda = 580$  nm is characteristic of the cationic radical of TPPy (TPPy $^{\bullet+}$ ), which was confirmed by UV–vis spectroscopy of chemically oxidized TPPy with  $\text{SbCl}_5$  (Figure S6 of the Supporting Information). The time profiles of the transient absorption intensities at  $\lambda = 580$  and 740 nm exhibited a rise and a decay, respectively, with a similar time constant (inset of Figure 9). These results indicate that the photo-induced electron transfer from the TPPy bridging groups to excited dye 4 occurred in the P123–TPPy/4 film, which suggests that a close host–guest arrangement is realized in the film. Generation of the radicals occurred within ca. 100 ps, and the resultant charge-separated state was retained over a nanosecond time scale.

The dispersion states of the PBI dyes 1–4 in the mesochannels are summarized in Figure 10a. The appropriate

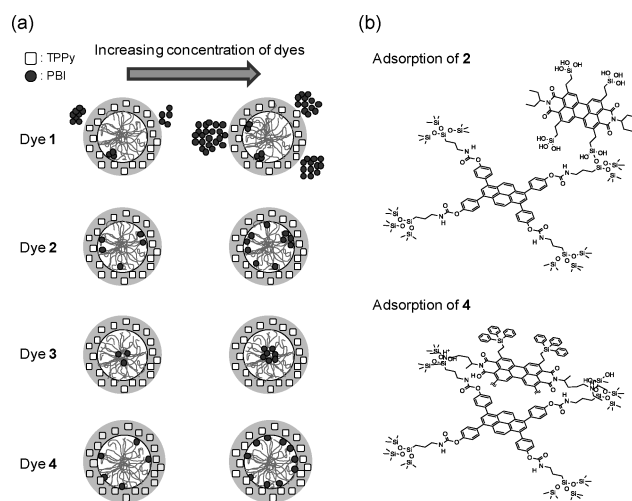


**Figure 10.** (a) Schematic illustration of the distribution of PBI dyes in the mesochannel. (b) Plausible scheme for the adsorption of dyes 2 and 4 onto the TPPy–silica framework.

selection of substituents ( $R^1$  and  $R^2$ ) enabled control of the location and dispersion of the dye molecules. Dye 1 with a linear  $R^1$  group is not easily dispersed in the mesostructured films because of strong self-aggregation. Dye 3, which is a bulky and entirely hydrophobic dye, is located in the center of the template surfactant micelles. In this case, the FRET efficiency is varied according to the dimension of the mesostructure that

determines the host–guest distance. This host–guest arrangement is useful in certain cases (e.g., photoluminescent materials), because undesired electron transfer is completely suppressed as a result of the isolation of donors and acceptors. Dyes **2** and **4**, which have both polar anchoring groups for organosilica pore walls and bulky substituents to suppress self-aggregation, are appropriate for molecular-level dispersion of the dyes and inducing efficient host–guest interaction. Efficient FRET and fluorescence emission from the PBI dye were observed in the mesostructured TPPy–silica films containing dye **2**. In contrast, the TPPy–silica films containing dye **4** exhibited photo-induced electron transfer from the host TPPy to the guest PBI. The different energy and electron-transfer behavior between dyes **2** and **4** is attributable to the difference in the functionality of the polar substituents. The four trimethoxysilyl moieties of dye **2** not only function as an anchor to organosilica pore walls but also connect the PBI molecules to each other. In contrast, the protonated cationic amino groups of dye **4** strongly interact with the organosilica framework and also suppress dye aggregation by electrostatic repulsion, which results in monolayer adsorption of the dyes onto the surface of the TPPy–silica framework. The lengths of the polar substituents [ $-(\text{CH}_2)_2\text{Si}(\text{OH})_3$  for dye **2** and  $-\text{CH}(\text{CH}_3)(\text{CH}_2)_3\text{NH}^+\text{Et}_2$  for dye **4**] can also affect the TPPy–PBI interaction (Figure 10b). When the terminal polar groups anchor onto the silica moieties of the TPPy–silica pore wall, the PBI core of dye **4** can become closer to the TPPy unit than that of dye **2**, because the length of the polar substituent of dye **4** is similar to that of the  $-\text{CONH}(\text{CH}_2)_3-$  linker of TPPy–Si. The close proximity of the TPPy moiety and PBI core of dye **4** is conducive to photo-induced electron transfer.

## CONCLUSION

Systematic design of PBI dye-doped mesostructured TPPy–silica films led to fine-tuning of the energetic and electronic host–guest interactions. The location of the guest PBI dyes in the mesostructured films was dependent upon the chemical structure of the substituents. The combination of bulky substituents and polar anchoring groups proved effective to realize the molecular-level dispersion of guest dyes and a close host–guest arrangement, which resulted in efficient fluorescence quenching of the host TPPy units and energy/electron transfer from the pore walls to the guest dyes. Although a variety of FRET systems have been reported for zeolites,<sup>25</sup> micelles,<sup>26</sup> polymers,<sup>27</sup> dendrimers,<sup>28</sup> organogels,<sup>29</sup> etc., the molecular-level tunability of the host–guest arrangement shown in this work merits attention. The present design concept of the functional mesostructured materials containing photo- and electroactive organic guests with controlled distribution will be expanded to future applications, such as efficient photocatalytic systems and high-sensitivity molecular sensors.

## ASSOCIATED CONTENT

### Supporting Information

Supplementary spectroscopic data, XRD patterns, and calculation of the critical Förster radius. This material is available free of charge via the Internet at <http://pubs.acs.org>.

## AUTHOR INFORMATION

### Corresponding Author

\*E-mail: [inagaki@mosk.tytlabs.co.jp](mailto:inagaki@mosk.tytlabs.co.jp).

## Notes

The authors declare no competing financial interest.

## REFERENCES

- (1) Hoffmann, F.; Cornelius, M.; Morell, J.; Fröba, M. *Angew. Chem., Int. Ed.* **2006**, *45*, 3216–3251.
- (2) Wang, W.; Lofgreen, J. E.; Ozin, G. A. *Small* **2010**, *6*, 2634–2642.
- (3) Mizoshita, N.; Tani, T.; Inagaki, S. *Chem. Soc. Rev.* **2011**, *40*, 789–800.
- (4) Inagaki, S.; Guan, S.; Fukushima, Y.; Ohsuna, T.; Terasaki, O. *J. Am. Chem. Soc.* **1999**, *121*, 9611–9614.
- (5) Melde, B. J.; Holland, B. T.; Blanford, C. F.; Stein, A. *Chem. Mater.* **1999**, *11*, 3302–3308.
- (6) Asefa, T.; MacLachlan, M. J.; Coombs, N.; Ozin, G. A. *Nature* **1999**, *402*, 867–871.
- (7) Yoshina-Ishii, C.; Asefa, T.; Coombs, N.; MacLachlan, M. J.; Ozin, G. A. *Chem. Commun.* **1999**, 2539–2540.
- (8) Inagaki, S.; Ohtani, O.; Goto, Y.; Okamoto, K.; Ikai, M.; Yamanaka, K.; Tani, T.; Okada, T. *Angew. Chem., Int. Ed.* **2009**, *48*, 4042–4046.
- (9) Takeda, H.; Goto, Y.; Maegawa, Y.; Ohsuna, T.; Tani, T.; Matsumoto, K.; Shimada, T.; Inagaki, S. *Chem. Commun.* **2009**, 6032–6034.
- (10) Mizoshita, N.; Goto, Y.; Tani, T.; Inagaki, S. *Adv. Mater.* **2009**, *21*, 4798–4801.
- (11) Mizoshita, N.; Goto, Y.; Maegawa, Y.; Tani, T.; Inagaki, S. *Chem. Mater.* **2010**, *22*, 2548–2554.
- (12) Maegawa, Y.; Mizoshita, N.; Tani, T.; Inagaki, S. *J. Mater. Chem.* **2010**, *20*, 4399–4403.
- (13) Ohashi, M.; Aoki, M.; Yamanaka, K.; Nakajima, K.; Ohsuna, T.; Tani, T.; Inagaki, S. *Chem.—Eur. J.* **2009**, *15*, 13041–13046.
- (14) Takeda, H.; Ohashi, M.; Tani, T.; Ishitani, O.; Inagaki, S. *Inorg. Chem.* **2010**, *49*, 4554–4559.
- (15) Yamaguchi, A.; Amino, Y.; Shima, K.; Suzuki, S.; Yamashita, T.; Teramae, N. *J. Phys. Chem. B* **2006**, *110*, 3910–3916.
- (16) (a) Minoofar, P. N.; Dunn, B. S.; Zink, J. I. *J. Am. Chem. Soc.* **2005**, *127*, 2656–2665. (b) Johansson, E.; Zink, J. I. *J. Am. Chem. Soc.* **2007**, *129*, 14437–14443.
- (17) (a) Wicklein, A.; Lang, A.; Muth, M.; Thelakkt, M. *J. Am. Chem. Soc.* **2009**, *131*, 14442–14453. (b) Würthner, F. *Pure Appl. Chem.* **2006**, *78*, 2341–2349. (c) Würthner, F.; Stolte, M. *Chem. Commun.* **2011**, *47*, 5109–5115. (d) Kaiser, T. E.; Wang, H.; Stepanenko, V.; Würthner, F. *Angew. Chem., Int. Ed.* **2007**, *46*, 5541–5544. (e) Baram, J.; Shirman, E.; Ben-Shitrit, N.; Ustinov, A.; Weissman, H.; Pinkas, I.; Wolf, S. G.; Rybtchinski, B. *J. Am. Chem. Soc.* **2008**, *130*, 14966–14967.
- (18) (a) Nakazono, S.; Imazaki, Y.; Yoo, H.; Yang, J.; Sasamori, T.; Tokitoh, N.; Cédric, T.; Kageyama, H.; Kim, D.; Shinokubo, H.; Osuka, A. *Chem.—Eur. J.* **2009**, *15*, 7530–7533. (b) Nakazono, S.; Easwaramoorthi, S.; Kim, D.; Shinokubo, H.; Osuka, A. *Org. Lett.* **2009**, *11*, 5426–5429. (c) Teraoka, T.; Hiroto, S.; Shinokubo, H. *Org. Lett.* **2011**, *13*, 2532–2535.
- (19) Yamaguchi, S.; Hamaguchi, H. *Appl. Spectrosc.* **1995**, *49*, 1513–1515.
- (20) (a) Tang, T.; Herrmann, A.; Peneva, K.; Müllen, K.; Webber, S. E. *Langmuir* **2007**, *23*, 4623–4628. (b) Baumann, J.; Fayer, M. D. *J. Chem. Phys.* **1986**, *85*, 4087–4107.
- (21) Similar fluorescence quenching of both host and guest chromophores was also observed for Brij76–TPPy films doped with dye **4** (data not shown).
- (22) The P123–silica film was prepared from 200 mg of P123 and 300 mg of tetraethoxysilane, using the similar procedure to that used for the preparation of the organosilica films.
- (23) Hippus, C.; van Stokkum, I. H. M.; Zangrando, E.; Williams, R. M.; Würthner, F. *J. Phys. Chem. C* **2007**, *111*, 13988–13996.
- (24) In the P123–TPPy/4 (10 mol %) film, a part of the dye molecules can form dimers or aggregates because of the excessive doping. The aggregates of dye **4** turned out to exhibit a transient absorption band at  $\lambda = 765$  nm from the time-resolved absorption

spectra of a P123–silica/4 film (P123/4 = 100:8.7, w/w). See Figures S7 and S8 of the Supporting Information.

(25) Brühwiler, D.; Calzaferri, G.; Torres, T.; Ramm, J. H.; Gartmann, N.; Dieu, L.-Q.; López-Duarte, I.; Martínez-Díaz, M. V. *J. Mater. Chem.* **2009**, *19*, 8040–8067.

(26) Grandini, P.; Mancin, F.; Tecilla, P.; Scrimin, P.; Tonellato, U. *Angew. Chem., Int. Ed.* **1999**, *38*, 3061–3064.

(27) (a) Thomas, S. W.; Joly, G. D.; Swager, T. M. *Chem. Rev.* **2007**, *107*, 1339–1386. (b) Méallet-Renault, R.; Pansu, R.; Amigoni-Gerbier, S.; Larpent, C. *Chem. Commun.* **2004**, 2344–2345.

(28) D'Ambruoso, G. D.; McGrath, D. V. *Adv. Polym. Sci.* **2008**, *214*, 87–147.

(29) (a) Ajayaghosh, A.; Praveen, V. K.; Vijayakumar, C. *Chem. Soc. Rev.* **2008**, *37*, 109–122. (b) Babu, S. S.; Kartha, K. K.; Ajayaghosh, A. *J. Phys. Chem. Lett.* **2010**, *1*, 3413–3424. (c) Ajayaghosh, A.; Vijayakumar, C.; Praveen, V. K.; Babu, S. S.; Varghese, R. *J. Am. Chem. Soc.* **2006**, *128*, 7174–7175. (d) Ajayaghosh, A.; Praveen, V. K.; Vijayakumar, C.; George, S. J. *Angew. Chem., Int. Ed.* **2007**, *46*, 6260–6265.